Electronic Supplementary Material (ESI) for Lab on a Chip.

Supplementary Information:

A Rapid and Low-cost Fabrication and Integration Scheme to Render 3D Microfluidic Architectures for Wearable Biofluid Sampling, Manipulation, and Sensing

Haisong Lin[1], Yichao Zhao[1,2], Shuyu Lin[1], Bo Wang[1], Christopher Yeung[1,2], Xuanbing Cheng[1,2], Zhaoqing Wang[1], Tianyou Cai[1], Wenzhuo Yu[1], Kimber King[1], Jiawei Tan[1,2], Kamyar Salahi[1], Hannaneh Hojaiji[1], and Sam Emaminejad[1]*

[1] Department of Electrical and Computer Engineering, University of California, Los Angeles, CA, USA

[2] Department of Materials Science and Engineering, University of California, Los Angeles, CA, USA

* Correspondence and requests for materials should be addressed to S.E. (emaminejad@ucla.edu)

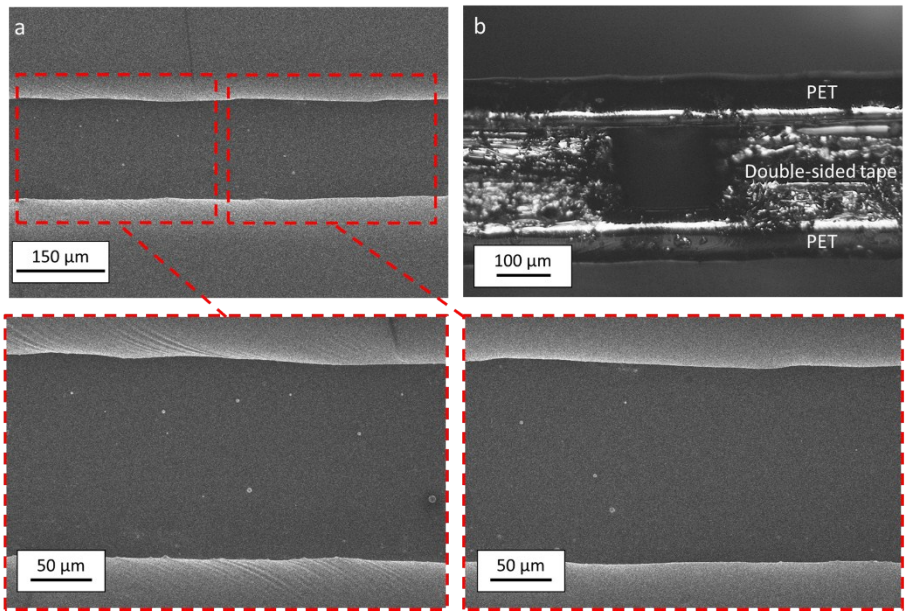

Supplementary Fig. 1: a) SEM images of the laser-cut tape-based microchannel (top view, microchannel bottom is PET and walls are double-sided tape) with corresponding zoomed-in images outlined. b) Optical microscope image of the cross section view of the laser-cut tape-based channel.

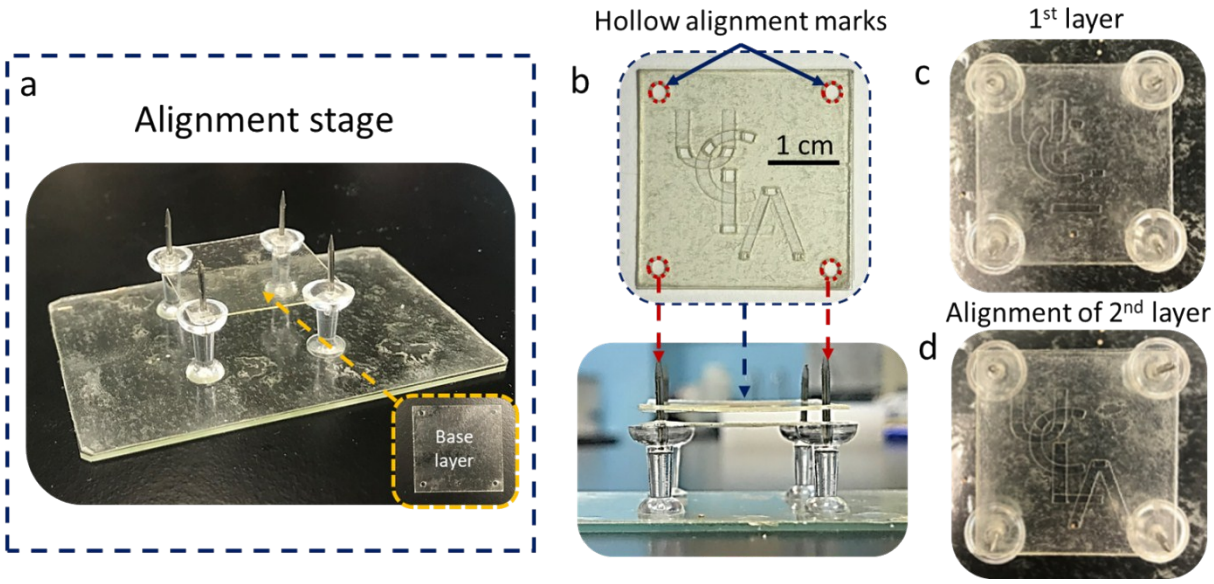

Supplementary Fig. 2: a,b) Alignment procedure for vertical device assembly with the aid of hollow alignment markers. The stage (a) consists of a laser-cut "base" layer (a, inset) with 4 hollow alignment markers (b), which is pushed through four posts (pins). This stage allows for the alignment of the subsequent layers (which are also laser cut with hollow alignment markers at the same positions), by simply pushing the layers through the posts. c,d) Assembly of an illustrative 3D microfluidic device. Alignment of the first layer (c) and second layer (d), both containing laser-patterned microfluidic features which form a 3D microfluidic device upon assembly.

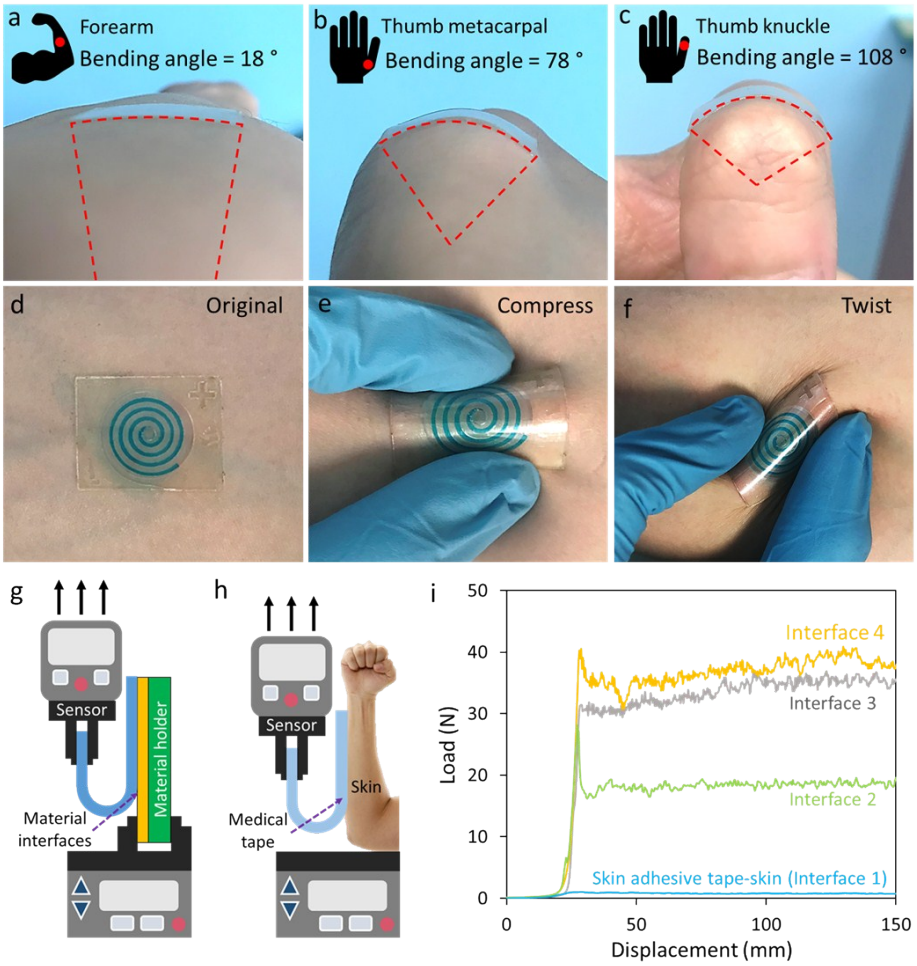

Supplementary Fig. 3: On-body bending test of an illustrative multilayered device (composed of PET/double-sided tape/skin adhesive medical tape layers) on different body parts: a) forearm, b) thumb metacarpal, and c) thumb knuckle with bending angles of a) 18°, b) 78°, and c) 108°, respectively. Conformal device-skin adherence under different conditions: d) no strain, e) compressing, and f) twisting. g) 180° peeling adhesion force characterization setup using Instron 5943 for different material interfaces (used in device construction). h) 180° peeling adhesion force characterization setup using Instron 5943 for the skin-skin adhesive medical tape interface. i) Force characterization results (device displacement rate: 5 mm/s, material peeling width: 3 cm). Interface 1: skin adhesive medical tape and skin. Interface 2: double-sided tape and skin adhesive medical tape. Interface 3: double-sided tape and PET. Interface 4: double-sided tape and double-sided tape.

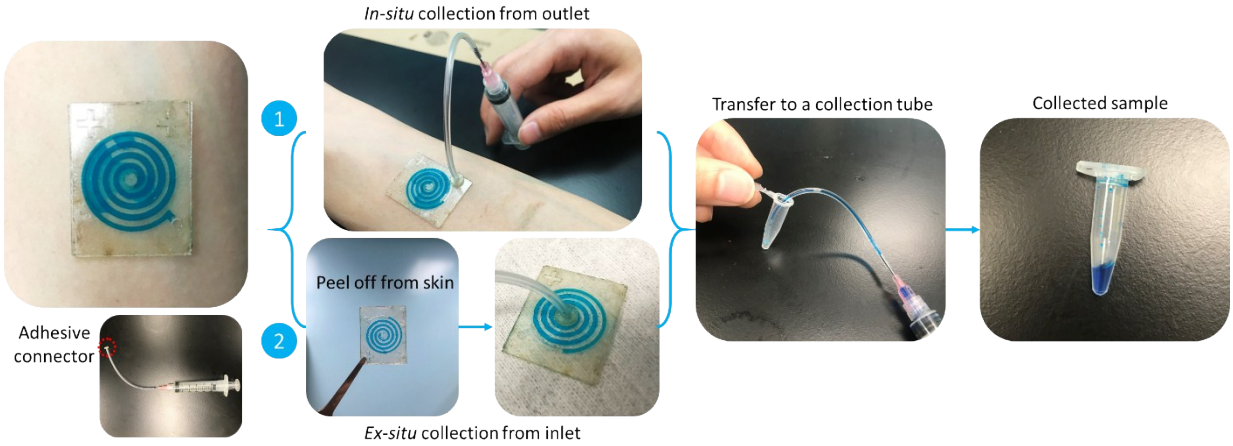

Supplementary Fig. 4: Demonstration of two sweat sample collection and transfer processes with the aid of the sweat collection device and a syringe with an adhesive-connector: 1) *In-situ* collection directly from the device while it is attached on-body. 2) *Ex-situ* collection with the device after removed from the body.

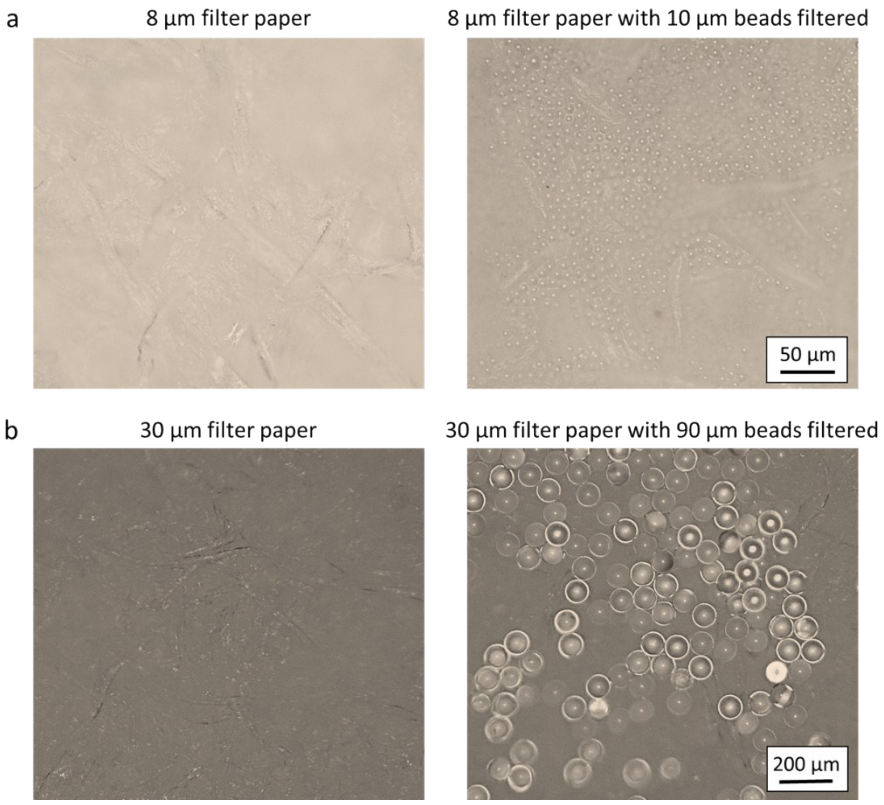

Supplementary Fig. 5: Optical microscope images of a) 8 µm filter paper before and after filtration of 10 µm beads, and b) 30 µm filter paper before and after filtration of 90 µm beads.

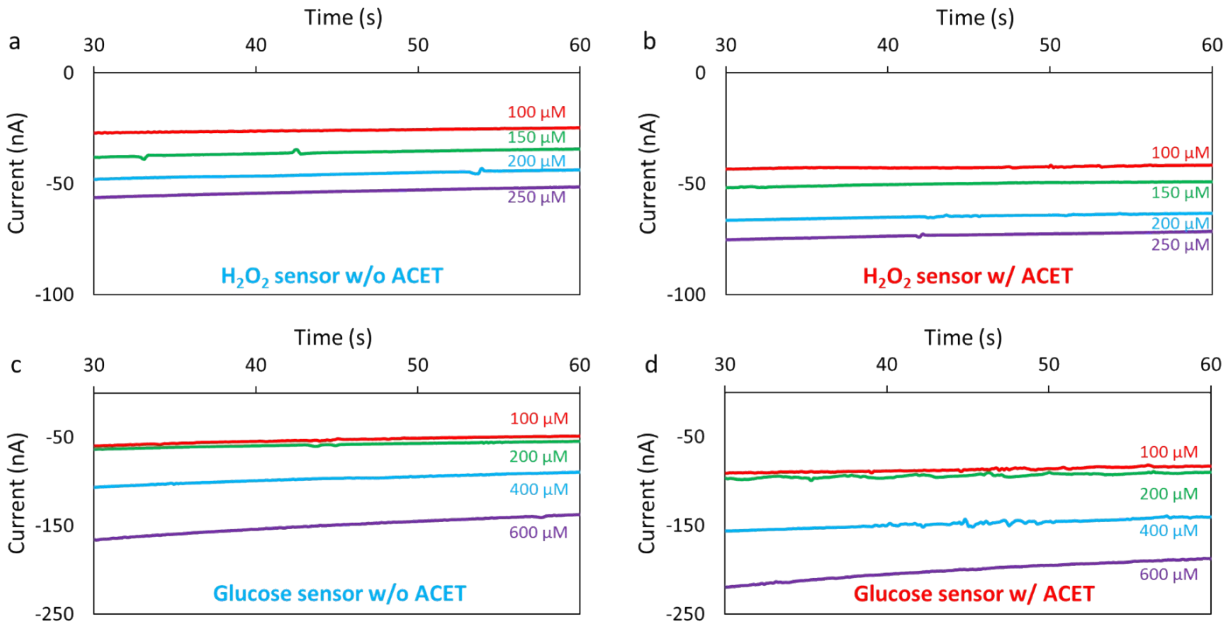

Supplementary Fig. 6: Recordings of the sensor steady-state responses shown in Fig. 4d,e: a) H_2O_2 without ACET actuation, b) H_2O_2 with ACET actuation, c) Glucose without ACET actuation, and d) Glucose with ACET actuation.

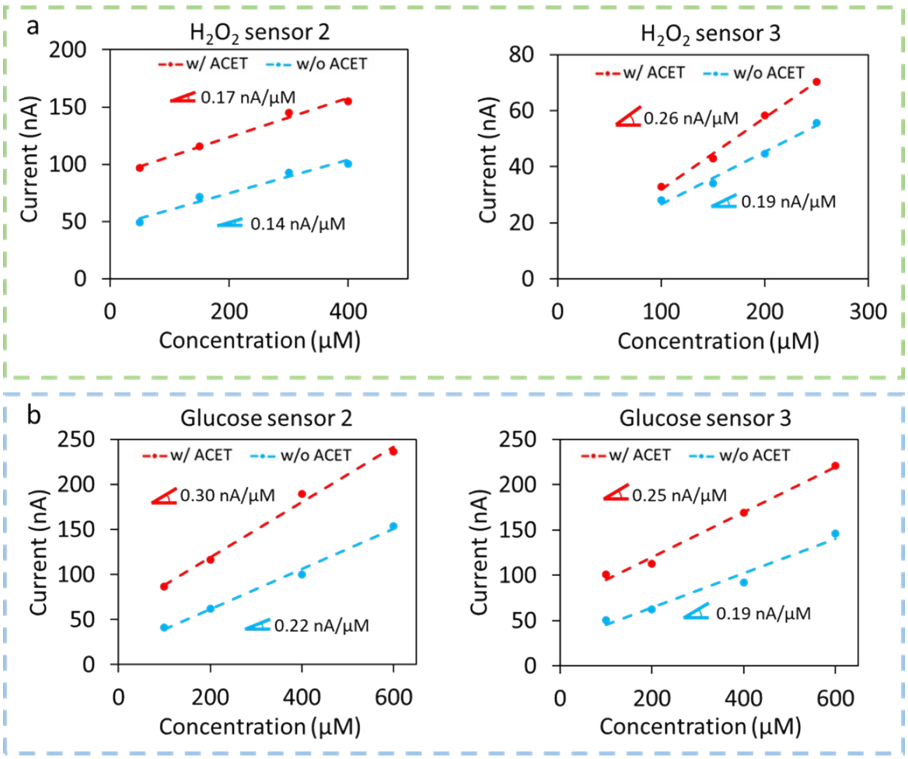

Supplementary Fig. 7: Reproduced sensor calibration results with and without ACET actuation: a) H_2O_2 sensor response and b) Glucose sensor response.

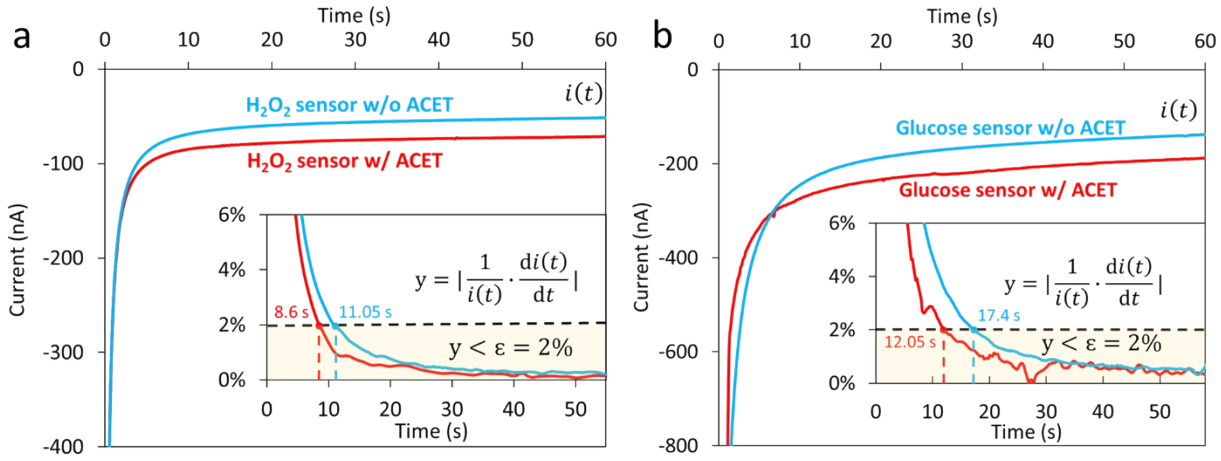

Supplementary Fig. 8: Recordings of the H_2O_2 (a) and glucose (b) sensors' amperometric responses with and without the presence of ACET. The corresponding insets show the normalized slope functions (see Materials and method section) for the determination of the sensors' response times.

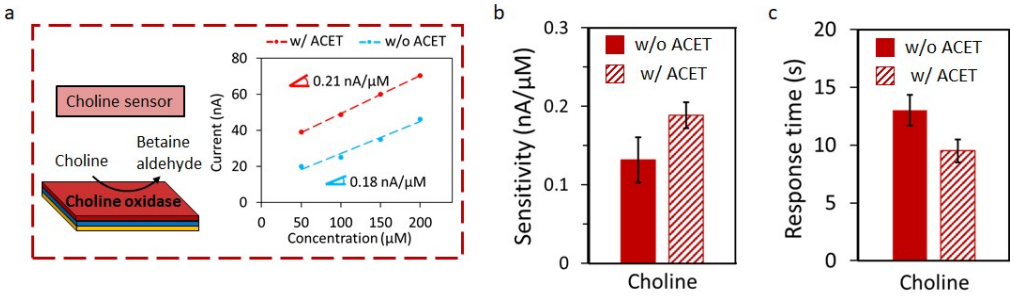

Supplementary Fig. 9: a) Enzymatic choline sensing mechanism and representative calibration curves of the sensor response (with and without ACET actuation). b, c) Comparison of choline sensor's sensitivity (b) and response time (c) for the cases of with and without ACET actuation (error bars indicate standard error, N = 3).